

# An Improved Exact Riemann Solver for Multidimensional Relativistic Flows

By **LUCIANO REZZOLLA**<sup>1,2</sup>, **OLINDO ZANOTTI**<sup>1</sup> AND **JOSE A. PONS**<sup>3</sup>

<sup>1</sup> SISSA, International School for Advanced Studies, Trieste, Via Beirut 2–4, 34014 Trieste, Italy

<sup>2</sup> INFN, Physics Department, University of Trieste, Via Valerio 2, 34127 Trieste, Italy

<sup>3</sup> Physics Department, University of Rome “La Sapienza”, Piazzale Aldo Moro 2, I-00185 Rome, Italy

(Received 29 October 2018)

We extend our approach for the exact solution of the Riemann problem in relativistic hydrodynamics to the case in which the fluid velocity has components tangential to the initial discontinuity. As in one-dimensional flows, we here show that the wave-pattern produced in a multidimensional relativistic Riemann problem can be predicted entirely by examining the initial conditions. Our method is logically very simple and allows for a numerical implementation of an exact Riemann solver which is both straightforward and computationally efficient. The simplicity of the approach is also important for revealing special relativistic effects responsible for a smooth transition from one wave-pattern to another when the tangential velocities in the initial states are suitably varied. While the content of this paper is focussed on a flat spacetime, the local Lorentz invariance allows its use also in fully general relativistic calculations.

---

## 1. Introduction

Since the solution of the Riemann problem has been introduced in numerical hydrodynamics (Godunov 1959), high resolution shock capturing methods have become a common tool for handling nonlinear hydrodynamical waves in a variety of physical situations and the subject of detailed mathematical analyses both in Newtonian (Leveque 1992, Toro 1997) and relativistic regimes (Smoller & Temple 1993). Nonlinear waves of this type are very common in astrophysical scenarios (such as gamma-ray bursts, accretion onto compact objects, relativistic jets, supernova explosions) in which the motion of the fluid is characterised by relativistic speeds and by the appearance of strong discontinuities (see Ibañez & Martí, 1999 and Martí & Müller, 1999 for a review). In a recent paper, Rezzolla & Zanotti (2001, hereafter paper I) have proposed a new procedure for the exact solution of the Riemann problem which uses the relativistically invariant relative velocity between the unperturbed “left” and “right” states of the fluid in order to extract important information contained in the initial data and that more traditional approaches were not able to put into evidence. Most notably, it was shown that, given a Riemann problem with assigned initial conditions, it is possible to determine in advance both the wave-pattern that will be produced after the removal of the initial planar discontinuity and the bracketing interval of the unknown pressure in the region that forms behind the wave fronts. Besides clarifying some aspects of the Riemann problem, the approach proposed by Rezzolla & Zanotti, and that was foreseen by Landau & Lifshitz (1959) in Newtonian hydrodynamics, was shown to be computationally more efficient as compared to the more traditional ones.

In a recent work, Pons *et al* (2000) have extended the analytic solution of the one-dimensional Riemann problem (Martí & Müller 1994) to the case in which nonzero velocities tangential to the initial planar discontinuity are present. An important result obtained by Pons *et al* (2000)

was to show that the introduction of tangential velocities and the appearance of global Lorentz factors linking quantities on either side of the discontinuity can affect the solution of the Riemann problem considerably. In the present paper we show that the approach by Rezzolla & Zanotti can be successfully extended to this more general case and with the same advantages that were found in the case of zero tangential velocities. Within this new procedure, the introduction of tangential velocities is imprinted in the expression for the jump of the velocity normal to the discontinuity surface, and this has allowed us to reveal interesting special relativistic effects. In relativistic hydrodynamics, in fact, the wave-pattern produced by the decay of the initial discontinuity can be changed by simply varying the tangential velocities in the initial states, while keeping the rest of the thermodynamic quantities of the Riemann problem unmodified. This effect has no analogue in Newtonian hydrodynamics (Rezzolla & Zanotti 2002).

The plan of the paper is as follows: after a review of the method in Section 2, we report in Section 3 the hydrodynamical equations relevant for the present discussion of nonzero tangential velocities. In Section 4 we show how to use the invariant relative velocity to extract from the initial data the information on the wave-pattern produced, while Section 5 is devoted to the presentation of the special relativistic effects. The conclusions of the paper are in Section 6, and two Appendices complete the discussion providing the mathematical details of the results obtained in the main text.

We use in this paper a system of units in which  $c = 1$ , a space-like signature  $(-, +, +, +)$  and a Cartesian coordinate system  $(t, x, y, z)$ . Greek indices are taken to run from 0 to 3, Latin indices from 1 to 3 and we adopt the standard convention for the summation over repeated indices.

## 2. A brief review of the method

In a flat spacetime consider a perfect fluid described by the stress-energy tensor:

$$T^{\mu\nu} \equiv (e + p)u^\mu u^\nu + p\eta^{\mu\nu} = \rho h u^\mu u^\nu + p\eta^{\mu\nu}, \quad (2.1)$$

where  $\eta^{\mu\nu} = \text{diag}(-1, 1, 1, 1)$  and  $e$ ,  $p$ ,  $\rho$ , and  $h$  are the proper energy density, the isotropic pressure, the proper rest mass density, and the specific enthalpy, respectively.

Further assume the fluid to consist of an initial “left” state (indicated with an index 1) and an initial “right” state (indicated with an index 2), each having prescribed and different values of uniform pressure, rest-mass density and velocity. The two discontinuous states are initially separated by a planar surface  $\Sigma_0$  placed at a constant value of the  $x$  coordinate so that the unit space-like 4-vector  $n_0^\mu$  normal to this surface at  $t = 0$  has components  $n_0^\mu \equiv (0, 1, 0, 0)^\dagger$ . Because we are considering a multidimensional flow, the fluid 4-velocity on either side of the initial discontinuity is allowed to have components in spatial directions orthogonal to  $n_0^\mu$ , i.e.

$$u^\mu \equiv W(1, v^x, v^y, v^z), \quad (2.2)$$

where  $W^2 = (1 - v^2)^{-1}$  is the square of the Lorentz factor and  $v^2 \equiv v^i v_i = (v^x)^2 + (v^y)^2 + (v^z)^2$  is the norm of the 3-velocity. The hydrodynamical properties of the initial left and right states are described by the “state-vectors”

$$\mathbf{U}_{1,2} = \begin{pmatrix} p \\ \rho \\ v^x \\ v^t \end{pmatrix}_{1,2},$$

where we have indicated with  $v^t \equiv [(v^y)^2 + (v^z)^2]^{1/2}$  the *tangential* component of the three

† More precisely, the unit normal to the hypersurface  $\Sigma_0$  is defined as the one-form mapping each vector tangent to the surface into zero.

velocity, satisfying the obvious relativistic constraint that  $(v^t)^2 + (v^x)^2 \leq 1$  (Note that in paper I the 4-velocity vector was chosen so that  $v^y = v^z = 0 = v^t$ ). Hereafter, we will refer to  $v^x$  as the *normal* velocity.

The fluid states  $\mathbf{U}_1$  and  $\mathbf{U}_2$  represent the initial conditions of a multidimensional ‘‘Riemann problem’’ whose solution consists of determining the flow that develops when the system is allowed to relax. In general, the temporal evolution can be indicated as (Martí & Müller 1994)

$$L\mathcal{W}_{\leftarrow}L_*\mathcal{C}R_*\mathcal{W}_{\rightarrow}R, \quad (2.3)$$

where  $\mathcal{W}$  denotes a nonlinear wave (either a shock,  $\mathcal{S}$ , or a rarefaction wave,  $\mathcal{R}$ ), propagating towards the left ( $\leftarrow$ ) or the right ( $\rightarrow$ ) with respect to the initial discontinuity. Moreover,  $L_*$  and  $R_*$  are the new hydrodynamic states that form behind the two nonlinear waves propagating in opposite directions. A contact discontinuity,  $\mathcal{C}$ , separates the region  $L_*$  and  $R_*$ , and it is characterised by the fact that both the pressure and the normal velocity are continuous across it, while both the rest-mass density and the tangential velocities can be discontinuous.

The approach introduced in paper I focuses on  $(v_{12}^x)_0$ , the relativistic invariant expression for the relative velocity between the two unperturbed initial states. By construction, this quantity measures the relativistic jump of the fluid velocity normal to the discontinuity surface. The solution of the relativistic Riemann problem is then found after the pressure in the region between the two nonlinear waves,  $p_*$ , is calculated as the root of the nonlinear equation

$$v_{12}^x(p_*) - (v_{12}^x)_0 = 0, \quad (2.4)$$

where  $v_{12}^x(p_*)$  has a functional form that is *different* for each of the *three* possible wave-patterns that might result from the decay of the initial discontinuity. The key aspect of the new approach is that the wave-pattern produced by the decay of the initial discontinuity can be entirely predicted in terms of the initial data  $\mathbf{U}_{1,2}$ . This represents an important advantage since it allows to deduce in advance which set of equations to use for the solution of the exact Riemann problem and the interval bracketing the root of (2.4).

The validity of the approach discussed in paper I is in the mathematical proof that the function  $v_{12}^x = v_{12}^x(p_*)$  is monotonically increasing with  $p_*$  and it is composed of three branches corresponding to the three possible wave-patterns. Furthermore, the three different branches always join smoothly through specific values of  $v_{12}^x(p_*)$ , denoted respectively as  $(\tilde{v}_{12}^x)_{2S}$ ,  $(\tilde{v}_{12}^x)_{SR}$ ,  $(\tilde{v}_{12}^x)_{2R}$ † (cf. Fig. 1 of paper I). In view of these properties, it is possible to compare  $(v_{12}^x)_0$  with the relevant limiting values  $(\tilde{v}_{12}^x)_{2S}$ ,  $(\tilde{v}_{12}^x)_{SR}$ ,  $(\tilde{v}_{12}^x)_{2R}$  constructed from the initial conditions and determine, prior to the solution of equation (2.4), both the wave-pattern that will be produced and the functional form of  $v_{12}^x(p_*)$  to be used. The logical scheme to be followed in this procedure is synthesised as follows

$$\begin{array}{lll} (v_{12}^x)_0 > (\tilde{v}_{12}^x)_{2S} : & LS_{\leftarrow}L_*\mathcal{C}R_*\mathcal{S}_{\rightarrow}R & v_{12}^x(p_*) = (v_{12}^x)_{2S} \\ (\tilde{v}_{12}^x)_{SR} < (v_{12}^x)_0 \leq (\tilde{v}_{12}^x)_{2S} : & LR_{\leftarrow}L_*\mathcal{C}R_*\mathcal{S}_{\rightarrow}R, & v_{12}^x(p_*) = (v_{12}^x)_{SR} \\ (\tilde{v}_{12}^x)_{2R} < (v_{12}^x)_0 \leq (\tilde{v}_{12}^x)_{SR} : & LR_{\leftarrow}L_*\mathcal{C}R_*\mathcal{R}_{\rightarrow}R, & v_{12}^x(p_*) = (v_{12}^x)_{2R} \\ (v_{12}^x)_0 \leq (\tilde{v}_{12}^x)_{2R} : & LR_{\leftarrow}L_*\mathcal{C}R_*\mathcal{R}_{\rightarrow}R \text{ with vacuum,} & - \end{array} \quad (2.5)$$

After the initial relative normal-velocity  $(v_{12}^x)_0$  has been compared with the limiting values for the different branches and the correct wave-pattern [i.e. the functional form  $v_{12}^x(p_*)$ ] has been found, the numerical solution of the exact Riemann problem can be performed. Furthermore, the knowledge of the wave-pattern relevant for the solution of the problem provides the values

† Here  $2S$ ,  $SR$  and  $2R$  indicate a two shock, a shock-rarefaction and a two rarefaction wave-pattern, respectively.

$p_{\max}$  and  $p_{\min}$  bracketing the unknown pressure  $p_*$ . In the case of a one-dimensional flow, the bracketing interval is synthesized in the scheme below

	$LS_{\leftarrow}L_*CR_*S_{\rightarrow}R$	$LR_{\leftarrow}L_*CR_*S_{\rightarrow}R$	$LR_{\leftarrow}L_*CR_*R_{\rightarrow}R$
$p_{\min}$	$\max(p_1, p_2)$	$\min(p_1, p_2)$	0
$p_{\max}$	$\infty$	$\max(p_1, p_2)$	$\min(p_1, p_2)$

In practice, this novel approach has two major advantages. Firstly, it results into a straightforward numerical implementation and in a more efficient numerical algorithm with a reduction of the computational costs. Secondly, it simplifies considerably the logic formulation of the relativistic Riemann problem. As we shall discuss in Section 5, this feature has been essential in revealing new special relativistic effects.

The extension of the approach presented in paper I to the case when tangential velocities are present is straightforward and equation (2.4) as well as the logical scheme (2.5) apply unmodified<sup>†</sup>. The only changes introduced by the presence of tangential velocities are restricted to the expressions for the limiting values of the relative velocity  $(\tilde{v}_{12}^x)_{2S}$ ,  $(\tilde{v}_{12}^x)_{SR}$ ,  $(\tilde{v}_{12}^x)_{2R}$ . The details of these changes will be presented in the following Sections which have been written for a generic equation of state (EOS) and use an ideal fluid EOS as a test case.

### 3. Hydrodynamical Relations across the waves

As discussed in the previous Section, the expression for the relative normal-velocity between the two initial states of the Riemann problem represents the building block in our approach and, to simplify our notation, hereafter we will refer to the different flow regions using the following mapping

$$LW_{\leftarrow}L_*CR_*W_{\rightarrow}R \quad \iff \quad 1W_{\leftarrow}3C3'W_{\rightarrow}2. \quad (3.1)$$

While the values of  $v_{12}^x$  are relativistic invariants, there exists a reference frame which is better suited to evaluate this quantity. In the reference frame of the contact discontinuity, in fact, the normal velocities behind the nonlinear waves are, by definition, zero (i.e.  $v_{3,C}^x = 0 = v_{3',C}^x$ ) and the relative velocities across the nonlinear waves measured in this reference frame will be

$$(v_{13}^x)_{,C} \equiv \frac{v_{1,C}^x - v_{3,C}^x}{1 - (v_{1,C}^x)(v_{3,C}^x)} = v_{1,C}^x, \quad (3.2)$$

$$(v_{23'}^x)_{,C} \equiv \frac{v_{2,C}^x - v_{3',C}^x}{1 - (v_{2,C}^x)(v_{3',C}^x)} = v_{2,C}^x. \quad (3.3)$$

Because of their invariance, the normal velocity jumps across the nonlinear waves measured in the Eulerian frame can be expressed as

$$(v_{13}^x) = \frac{v_1^x - v_3^x}{1 - v_1^x v_3^x} = (v_{13}^x)_{,C} = v_{1,C}^x, \quad (3.4)$$

<sup>†</sup> Note that in the case of two shock waves propagating in opposite directions the maximum value for the pressure needs not be infinite but can be determined from the solution of the equation  $v_{12}^x(p_*) - (v_{12}^x)_{\max} = 0$ , where  $(v_{12}^x)_{\max}$  is the maximum allowed value of the normal relative velocity that is compatible with the assigned initial tangential velocities.

$$(v_{23'}^x) = \frac{v_2^x - v_{3'}^x}{1 - v_2^x v_{3'}^x} = (v_{23'}^x)_{,C} = v_{2,C}^x. \quad (3.5)$$

As a result, the relative normal-velocity between the two initial states can be written as

$$v_{12}^x = (v_{12}^x)_{,C} = \frac{v_{1,C}^x - v_{2,C}^x}{1 - (v_{1,C}^x)(v_{2,C}^x)}. \quad (3.6)$$

In what follows we will briefly discuss how to calculate the normal-velocity jump across a shock wave and a rarefaction wave, respectively. The expressions derived in this way will then be used to calculate  $v_{1,C}^x$  and  $v_{2,C}^x$  necessary to build  $v_{12}^x = v_{12}^x(p_*)$  [cf. eq. (3.6)].

### 3.1. Jumps Across a Shock Wave

Following Pons *et al* (2000), we use the Rankine-Hugoniot conditions in the fixed Eulerian reference frame to express the normal velocity of the fluid on the back of the shock front in terms of the pressure<sup>†</sup>

$$v_b^x = \frac{h_a W_a v_a^x + W_s (p_b - p_a) / J}{h_a W_a + (p_b - p_a) [W_s v_a^x / J + 1 / (\rho_a W_a)]}, \quad (3.7)$$

where  $J$  is mass flux and the subscripts  $b$  and  $a$  denote a quantity evaluated on the back or ahead of the wave front, respectively. In equation (3.7),  $W_s \equiv (1 - V_s^2)^{-1/2}$  is the Lorentz factor of the shock velocity  $V_s$ , with the latter being

$$V_s^\pm = \frac{\rho_a^2 W_a^2 v_a^x \pm |J| \sqrt{J^2 + \rho_a^2 W_a^2 [1 - (v_a^x)^2]}}{\rho_a^2 W_a^2 + J^2}, \quad (3.8)$$

and with the  $\pm$  signs referring to a shock wave propagating to the right or to the left, respectively.

Besides giving the jump in the normal velocity across a shock wave, expression (3.7) states that the two regions of the flow across the shock wave are effectively coupled through a Lorentz factor which, we recall, is built also in terms of the tangential velocities. This is a purely relativistic feature and an important difference from Newtonian hydrodynamics, in which the solution of the Riemann problem does not depend on the tangential component of the flow. Many of the consequences introduced by this coupling will be further discussed in Section 5 but one of them can already be appreciated when looking at the jumps across the shock wave of the tangential velocities that can be written as

$$[[hWv^y]] = 0 = [[hWv^z]], \quad (3.9)$$

and where we have adopted the standard notation in which  $[[F]] \equiv F_a - F_b$  (Anile 1989). Conditions (3.9) basically state that the ratio  $v^y/v^z$  remains unchanged through rarefaction waves and therefore that the tangential velocity 3-vector does not rotate but can change its norm. This property, which applies also across rarefaction waves, represents a major difference from the behaviour of the tangential velocities across Newtonian nonlinear waves. In this latter case, in fact, the tangential velocity vector does not change its norm, nor rotates:  $[[v^y]] = 0 = [[v^z]]$ .

The square of the mass flux across the wave can be expressed as

$$J^2 = - \frac{[[p]]}{[[h/\rho]]}, \quad (3.10)$$

<sup>†</sup> Note that when tangential velocities are present, calculating jump conditions in the rest frame of the shock front is not particularly advantageous. In this case, in fact, the velocity jump across the shock cannot be expressed as an algebraic relation among the thermodynamical quantities across the shock [cf. eq. (3.1) of Rezzolla & Zanotti 2001]. Rather, the ratio of the velocities ahead and behind the shock front need to be found as root of a nonlinear equation. Analytic solutions to this equation can be found only in the *weak-shock* limit or for an ultrarelativistic equation of state (see Koenigl 1980 for a discussion).

where the ratio  $h/\rho$  in the shocked region can be calculated through the Taub adiabat (Taub, 1948)

$$[[h^2]] = \left( \frac{h_a}{\rho_a} + \frac{h_b}{\rho_b} \right) [[p]]. \quad (3.11)$$

In a general case, the mass flux can be obtained as a function of just one thermodynamical variable ( $p_*$ ) after using the EOS and the physical ( $h \geq 1$ ) solution of the nonlinear equation (3.11). In the case of an ideal fluid EOS,

$$p = (\gamma - 1)\rho\epsilon = k(s)\rho^\gamma, \quad (3.12)$$

where  $\gamma$  is the adiabatic index, and  $k(s)$  is the polytropic constant (dependent only on the specific entropy  $s$ ), this can be done explicitly because (3.10) and (3.11) take respectively the simple form

$$J^2 = -\frac{\gamma}{\gamma - 1} \frac{[[p]]}{[[h(h-1)/p]]}, \quad (3.13)$$

and

$$\left[ 1 + \frac{(\gamma - 1)(p_a - p_b)}{\gamma p_b} \right] h_b^2 - \frac{(\gamma - 1)(p_a - p_b)}{\gamma p_b} h_b + \frac{h_a(p_a - p_b)}{\rho_a} - h_a^2 = 0. \quad (3.14)$$

### 3.2. Jumps Across a Rarefaction Wave

When considering a rarefaction wave it is convenient to introduce the self-similar variable  $\xi \equiv x/t$  in terms of which similarity solutions to the hydrodynamical equations can be found. An explicit expression for  $\xi$  can be obtained by requiring that non-trivial similarity solutions for the rarefaction wave exist. This then yields (see Pons *et al* 2000 for details)

$$\xi = \frac{v^x(1 - c_s^2) \pm c_s \sqrt{(1 - v^2)[1 - v^2 c_s^2 - (v^x)^2(1 - c_s^2)]}}{1 - v^2 c_s^2}, \quad (3.15)$$

where here too the  $\pm$  signs correspond to rarefaction waves propagating to right or to the left, respectively. In the case of a perfect fluid, the isentropic character of the flow allows to calculate the velocity on the back of the wave as a solution of an ordinary differential equation

$$\frac{dv^x}{dp} = \frac{1}{\rho h W^2} \frac{(1 - \xi v^x)}{(\xi - v^x)}, \quad (3.16)$$

In principle, to calculate the normal fluid velocity at the tail of the rarefaction wave one should solve the ordinary differential equation (3.16), which might be very expensive numerically. To overcome this, it is convenient to make use of constraints such as those in expressions (3.9) (which remain valid also across a rarefaction wave) and express equation (3.16) in a different way. Defining  $\mathcal{A} \equiv h_a W_a v_a^t = h_b W_b v_b^t$ , the tangential velocity along a rarefaction wave can be expressed as

$$(v^t)^2 = \mathcal{A}^2 \left[ \frac{1 - (v^x)^2}{h^2 + \mathcal{A}^2} \right]. \quad (3.17)$$

This allows us to eliminate the dependence on  $v^t$  from equation (3.15). From the definition of the Lorentz factor and equation (3.17) it is straightforward to obtain

$$W^2 = \frac{h^2 + \mathcal{A}^2}{h^2(1 - (v^x)^2)}, \quad (3.18)$$

and after some algebra one can arrive at

$$\frac{(1 - \xi v^x)}{(\xi - v^x)} = \pm \frac{\sqrt{h^2 + \mathcal{A}^2(1 - c_s^2)}}{h c_s} \quad (3.19)$$

Using this results, equation (3.16) can be written as follows:

$$\frac{dv^x}{1 - (v^x)^2} = \pm \frac{\sqrt{h^2 + \mathcal{A}^2(1 - c_s^2)}}{(h^2 + \mathcal{A}^2)} \frac{dp}{\rho c_s}, \quad (3.20)$$

Note that in this way we have isolated the thermodynamical quantities on the right hand side of (3.20) and the kinematical ones on the left hand side, which can then be integrated analytically. For some particular cases (for example when the sound speed is constant), the right hand side too is integrable but for a generic EOS a numerical integration is necessary. The velocity at the tail of the rarefaction wave can then be obtained directly as

$$v_b^x = \tanh \mathcal{B}, \quad (3.21)$$

where

$$\mathcal{B} \equiv \frac{1}{2} \log \left( \frac{1 + v_a^x}{1 - v_a^x} \right) \pm \int_{p_a}^{p^*} \frac{\sqrt{h^2 + \mathcal{A}^2(1 - c_s^2)}}{(h^2 + \mathcal{A}^2)} \frac{dp}{\rho c_s} \quad (3.22)$$

Here,  $h = h(p, s)$ ,  $\rho = \rho(p, s)$ , and  $c_s = c_s(p, s)$ , and the isentropic character of rarefaction waves allows to fix  $s = s_a$ . Despite its complicated look, the integrand is a smooth, monotonic function of  $p$ , and a Gaussian quadrature with only 10-20 points has proved to be more accurate and efficient than a third order Runge-Kutta integrator requiring hundreds of function evaluations to solve (3.16). Testing and details on the numerical implementation of this procedure will be reported in a separate work.

A couple remarks should now be made about the flow properties of a multidimensional and relativistic Riemann problem. The first remark is about the flow conditions at the contact discontinuity where, as mentioned before, not only the rest-mass density but also the tangential velocities can be discontinuous. It is well known that under these conditions a Kelvin-Helmholtz (or shear-layer) instability could develop (Chandrasekhar, 1961), reach the nonlinear waves if these move subsonically and thus destroy the solution of the Riemann problem. While this could be a concern in principle, it is never a problem in practice. The reason for this is simple and is related to the fact that any implementation of an exact Riemann solver in a numerical code will provide the solution of the Riemann problem at a new time-level which is ‘‘Courant-Friedrichs-Lewy limited’’ from the previous one (Press *et al* 1986). Besides providing numerical stability, this time-step limitation also guarantees that the solution at the new time-level is everywhere causally connected with the one at the previous one. As a result, even if a Kelvin-Helmholtz instability would develop at the contact discontinuity propagating outward in the flow at the sound speed, this would not be able to influence the dynamics of the nonlinear waves over the time of interest in numerical calculations.

The second remark is about the presence of tangential velocities across a shock-wave which can be in general discontinuous. While the stability of relativistic planar shocks in one-dimensional flows has been the subject of several investigations in the past (Anile & Russo 1987a, 1987b, Anile 1989), very little if anything at all is known about the stability properties of shock waves with discontinuous tangential velocities. It is reasonable to expect that a nonzero mass flux across these discontinuities would stabilise them against the Kelvin-Helmholtz instability, but further work needs to be done in this direction before a conclusion can be drawn.

#### 4. Limiting relative velocities

As mentioned in the previous Sections, the basic operation in our approach consists of calculating the relative normal-velocity across the two initial states and comparing it with the limiting relative velocities for each of the three possible wave-patterns. In practice, this amounts to calculating equation (3.6) making use of expressions (3.4) and (3.5). In the following we will briefly

discuss the guidelines for the evaluation of the limiting relative velocities. In doing so we will adopt the convention of paper I and assume that  $p_1 > p_2$ , with the  $x$ -axis normal to the discontinuity surface being positively oriented from 1 to 2.

#### 4.1. 1 $\mathcal{S}_{\leftarrow}$ 3 $\mathcal{C}$ 3' $\mathcal{S}_{\rightarrow}$ 2: Two Shock Waves

We first consider a wave-pattern in which two shock waves propagate in opposite directions. In this case, the general expression for the relative normal-velocities between the two initial states  $(v_{12}^x)_{2S}$  can be calculated from (3.6) with the velocities behind the shock waves  $v_3^x$  and  $v_{3'}^x$  being determined through the jump condition (3.7). Because  $p_1$  is the smallest value that the pressure at the contact discontinuity  $p_3$  can take, the limiting value for the two shock waves branch  $(\tilde{v}_{12}^x)_{2S}$  can be expressed as

$$(\tilde{v}_{12}^x)_{2S} = \lim_{p_3 \rightarrow p_1} (v_{12}^x)_{2S} . \quad (4.1)$$

Evaluating the limit (4.1) basically involves calculating the limits of  $v_{1,C}^x$  and  $v_{2,C}^x$  for  $p_3$  tending to  $p_1$ . Both these limits are straightforward to calculate and are

$$\lim_{p_3 \rightarrow p_1} v_{1,C}^x = 0 , \quad (4.2)$$

$$\lim_{p_3 \rightarrow p_1} v_{2,C}^x = \frac{v_2^x - \bar{v}_{3'}^x}{1 - v_2^x \bar{v}_{3'}^x} , \quad (4.3)$$

where  $\bar{v}_{3'}^x$  is simply the value of  $v_{3'}^x$  for  $p_3 = p_1$ , i.e.

$$\bar{v}_{3'}^x \equiv \lim_{p_3 \rightarrow p_1} v_{3'}^x . \quad (4.4)$$

Using now the limits (4.2)–(4.3) and some lengthy but straightforward algebra, the explicit analytic expression for the limiting value of the two shock waves branch can be calculated as

$$(\tilde{v}_{12}^x)_{2S} = - \lim_{p_3 \rightarrow p_1} v_{2,C}^x = \frac{(p_1 - p_2)(1 - v_2^x \bar{V}_s)}{(\bar{V}_s - v_2^x)\{h_2 \rho_2 (W_2)^2 [1 - (v_2^x)^2] + p_1 - p_2\}} . \quad (4.5)$$

Here  $\bar{V}_s$  is the velocity of the shock wave propagating towards the right in the limit of  $p_3 \rightarrow p_1$  and an explicit expression for it can be found in Appendix B in the case of an ideal fluid. Expression (4.5) will be discussed further in Section 5 but it sufficient to point out here that the threshold value  $(\tilde{v}_{12}^x)_{2S}$  does not depend on the initial velocity in the state 1,  $v_1$ .

#### 4.2. 1 $\mathcal{R}_{\leftarrow}$ 3 $\mathcal{C}$ 3' $\mathcal{S}_{\rightarrow}$ 2: One Shock and one Rarefaction Wave

We next consider the wave-pattern consisting of a rarefaction wave propagating towards the left and of a shock wave propagating towards the right. Also in this case,  $(v_{12}^x)_{SR}$  can be calculated from (3.6) with  $v_{3'}^x$  being determined through the jump condition (3.7) and  $v_3^x$  from the numerical integration of equation (3.16) in the range  $[p_1, p_3]$ . Because  $p_2$  is now the lowest pressure in the unknown region behind the two nonlinear waves, the limiting value for the one shock and one rarefaction waves branch  $(\tilde{v}_{12}^x)_{SR}$  can be expressed as

$$(\tilde{v}_{12}^x)_{SR} = \lim_{p_3 \rightarrow p_2} (v_{12}^x)_{SR} . \quad (4.6)$$

In the limit  $p_3 \rightarrow p_2$ , the right-propagating shock is suppressed,  $v_{3'}^x \rightarrow v_2^x$  so that

$$\lim_{p_3 \rightarrow p_2} v_{2,C}^x = 0 , \quad (4.7)$$

and

$$(\tilde{v}_{12}^x)_{SR} = \lim_{p_3 \rightarrow p_2} v_{1,C}^x . \quad (4.8)$$



Defining now

$$\mathcal{B}_1 \equiv \frac{1}{2} \log \left( \frac{1 + v_1^x}{1 - v_1^x} \right), \quad (4.9)$$

and using (3.21), it is readily obtained that

$$(\tilde{v}_{12}^x)_{SR} = \lim_{p_3 \rightarrow p_2} \tanh(\mathcal{B}_1 - \mathcal{B}) = \tanh \left( \int_{p_1}^{p_2} \frac{\sqrt{h^2 + \mathcal{A}_1^2(1 - c_s^2)}}{(h^2 + \mathcal{A}_1^2)\rho c_s} dp \right), \quad (4.10)$$

where the above integral can be evaluated numerically. A better look at the integral shows that only quantities in the left state are involved (through the constant  $\mathcal{A}_1 \equiv h_1 W_1 v_1^t$ ) and that  $(\tilde{v}_{12}^x)_{SR}$  does not depend on the initial velocity in the state 2,  $v_2$ . This property has an important consequence that will be discussed in Section 5.

#### 4.3. 1 $\mathcal{R} \leftarrow$ 3 $\mathcal{C}$ 3' $\mathcal{R} \rightarrow$ 2: Two Rarefaction Waves

When the wave-pattern consists of two rarefaction waves propagating in opposite directions,  $(v_{12}^x)_{2R}$  can be calculated from (3.6) with the velocities behind the waves being calculated using (3.21) and (3.22). Since the lowest value of the pressure behind the tails of the rarefaction waves is zero, the limiting value for the two rarefaction waves branch  $(\tilde{v}_{12}^x)_{2R}$  is given by

$$(\tilde{v}_{12}^x)_{2R} = \lim_{p_3 \rightarrow 0} (v_{12}^x)_{2R}. \quad (4.11)$$

Proceeding as in previous subsection, we can now express  $(\tilde{v}_{12}^x)_{2R}$  as

$$(\tilde{v}_{12}^x)_{2R} = \frac{\bar{v}_{1,C}^x - \bar{v}_{2,C}^x}{1 - (\bar{v}_{1,C}^x)(\bar{v}_{2,C}^x)}, \quad (4.12)$$

where

$$\bar{v}_{1,C}^x = \tanh \left( \int_{p_1}^0 \frac{\sqrt{h^2 + \mathcal{A}_1^2(1 - c_s^2)}}{(h^2 + \mathcal{A}_1^2)\rho c_s} dp \right), \quad (4.13)$$

$$\bar{v}_{2,C}^x = \tanh \left( \int_0^{p_2} \frac{\sqrt{h^2 + \mathcal{A}_2^2(1 - c_s^2)}}{(h^2 + \mathcal{A}_2^2)\rho c_s} dp \right), \quad (4.14)$$

and where  $\mathcal{A}_2 \equiv h_2 W_2 v_2^t$ . While, the determination of  $(\tilde{v}_{12}^x)_{2R}$  requires the numerical calculation of the integrals (4.13) and (4.14), it has very little practical importance as it marks the transition to a wave-pattern with two rarefaction waves separated by vacuum; this is a very rare physical configuration which cannot be handled by a generic numerical code.

Note that in computing (4.12), both the left state quantities and the right ones are involved and, as a result,  $(\tilde{v}_{12}^x)_{2R}$  will depend on both  $v_1$  and  $v_2$ . This property will be important in the subsequent discussion in Section 5.

Fig. 1 shows the functional behaviour of  $v_{12}^x = v_{12}^x(p_3)$  and how this behaviour is changed by the presence of nonzero tangential velocities. The initial conditions are those of a modified Sod's problem (Sod, 1978) in which  $p_1 = 1.0$ ,  $\rho_1 = 1.0$ ,  $v_1^x = 0.0$ ,  $p_2 = 0.1$ ,  $\rho_2 = 0.125$ ,  $v_2^x = 0.0$ , and  $\gamma = 5/3$ . Each of the two curves shown is effectively the composition of three different ones (joined at the solid dots) corresponding to wave-patterns consisting of two shock waves (2S), one shock and one rarefaction wave (SR), and two rarefaction waves (2R). While the solid curve refers to initial conditions with zero tangential velocities, the dashed one is produced when nonzero tangential velocities,  $v_1^t = 0.7 = v_2^t$ , are considered. Note that also in this latter case, the three branches are monotonically increasing with  $p_3$  (a fundamental property whose mathematical proof can be found in Appendix A) but are all altered by the presence of nonzero tangential velocities. The consequences of this will be discussed in the next Section.

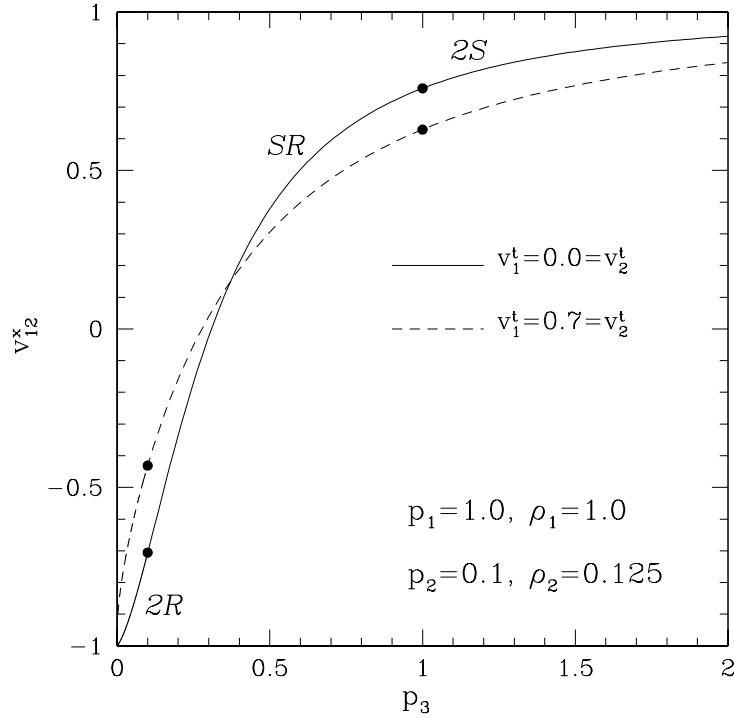


FIGURE 1. Relative normal-velocity between the two initial states as a function of the pressure at the contact discontinuity. Each curves is the continuous joining (marked by the solid dots) of three different curves corresponding respectively to two shock waves (2S), one shock and one rarefaction wave (SR), and two rarefaction waves (2R). The solid line refers to the case of zero tangential velocities, while the dashed line to the case in which  $v_1^t = 0.7 = v_2^t$ . The initial state vectors are those of Sod's problem.

## 5. Relativistic Effects

The changes in the functional behaviour of  $v_{12}^x = v_{12}^x(p_3)$  introduced by nonzero initial tangential velocities suggest that new qualitative differences could be found in a relativistic multidimensional Riemann problem. This was first discussed in a recent paper (Rezzolla & Zanotti 2002) where the basic features of new relativistic effects were briefly pointed out. This section is dedicated to a more detailed discussion of how the changes in the functional behaviour of  $v_{12}^x = v_{12}^x(p_3)$  are responsible for relativistic effects in the dynamics of nonlinear waves. Before entering in the heart of the discussion, however, it is useful to remind that in Newtonian hydrodynamics a multidimensional Riemann problem does not depend on the values of the tangential velocities in the two initial states. Rather, different wave-patterns can be produced only after a suitable change in either the normal velocity, the rest-mass density or the pressure. This is essentially due to the fact that tangential velocities are not changed across Newtonian nonlinear waves. In relativistic hydrodynamics, on the other hand, this is not the case and is at the origin of the effects discussed below.

Let us restrict our attention to a situation in which the tangential velocity of only one of the two initial states is varied. This is simpler than the general case as it basically represents a one-dimensional cross-section of the three-dimensional parameter space, but it maintains all of the relevant properties. The two panels of Fig. 2 show the relative normal-velocity for the same initial conditions of Fig. 1 where either  $v_1^t$  or  $v_2^t$  is varied while all the other quantities of the initial state vectors are left unchanged. Different line types mark the different branches (joined at the filled

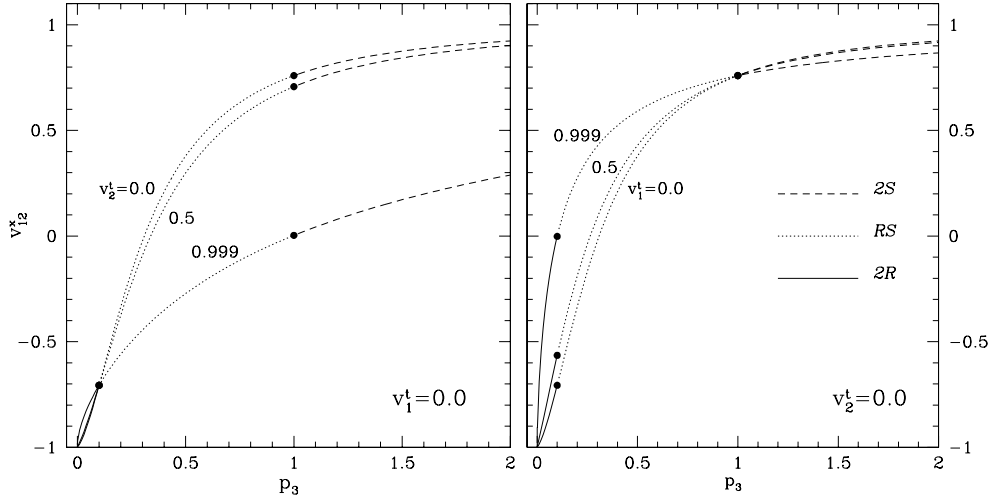


FIGURE 2. The same as in Fig. 1 but here the different line types mark the different branches corresponding to two shock waves (dashed line), one shock and one rarefaction wave (dotted line), and two rarefaction waves (continuous line), respectively. The two panels show how the functional behaviour is modified when only one of the initial tangential velocities is varied ( $v_2^t$  for the left panel and  $v_1^t$  for the right one) while all the other components of the initial state vectors are left unchanged.

dots) describing the relative velocity corresponding to two shock waves ( $2S$ , dashed line), one shock and one rarefaction wave ( $SR$ , dotted line), and two rarefaction waves ( $2R$ , continuous line), respectively. Both panels of Fig. 2 indicate that when tangential velocities are present the relative normal-velocity is a function of  $p_3$  but also of  $v_1^t$  and  $v_2^t$ †.

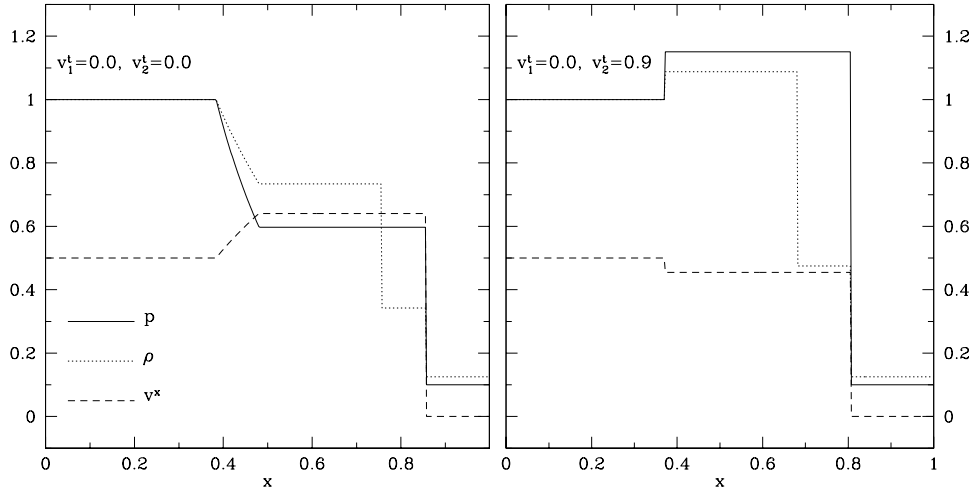


FIGURE 3. Transition from a  $SR$  wave-pattern to a  $2S$  one. The left and right panels show the exact solution of the Riemann problem corresponding to models (a) and (e) in Table I, respectively. The initial state vectors are identical except for the values of  $v_2^t$ . Solid, dotted and dashed profiles refer to pressure, rest-mass density and normal velocity, respectively.

† For the of initial conditions chosen in Fig. 2 the position of  $(\tilde{v}_{12})_{2R}$  is very close to the limit  $-1$ .

Consider, for instance, the case in which the normal velocities are chosen to be  $v_1^x = 0.5$ ,  $v_2^x = 0.0$ , and that there are no tangential velocities. In this case,  $(v_{12}^x)_0 = 0.5$  and the left panel of Fig. 2 shows that the solution to the Riemann problem falls in the  $SR$  branch, hence producing a wave-pattern consisting of a shock and a rarefaction wave moving in opposite directions. This is shown in more detail in the left panel of Fig. 3 where the different types of line show the solution of the Riemann problem at a time  $t > 0$  for the pressure (continuous line), the rest-mass density (dotted line) and the velocity (dashed line).

However, if we now maintain the *same* initial conditions but allow for nonzero tangential velocities in state 2, the left panel of Fig. 2 also shows that the solution to the Riemann problem can fall in the  $2S$  branch, hence producing a wave-pattern consisting of two shock waves moving in opposite directions. This is shown in the right panel of Fig. 3 which illustrates the solution of the same Riemann problem but with initial tangential velocities  $v_1^t = 0.0$  and  $v_2^t = 0.9$ . Note that except for the tangential velocities, the solutions in Figs. 3 have the same initial state-vectors but different intermediate ones (i.e.  $p_3$ ,  $\rho_3$ ,  $\rho_{3'}$ , and  $v_3^x$ ).

The Riemann problem shown in Fig. 3 is only one possible example but shows that a change in the tangential velocities can produce a *smooth transition from one wave-pattern to another while maintaining the initial states unmodified*. Furthermore, because the coupling among the different states is produced by the Lorentz factors this is not sensitive on the sign chosen for the tangential velocity. The transition from one wave-pattern to the other is better illustrated in Fig. 4 where we

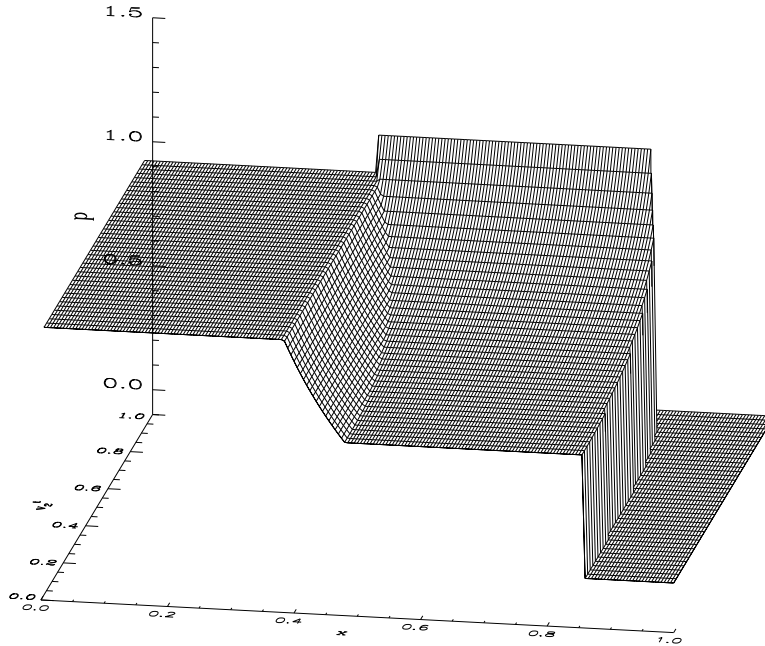


FIGURE 4. Sequence of solutions for the pressure in Sod's problem. The initial tangential velocity  $v_2^t$  is gradually increased from 0 to 0.9. The first and last solution of this sequence are also plotted in Fig. 3

have collected in a three-dimensional plot a sequence of solutions for the pressure in which  $v_2^t$  is gradually increased from 0 to 0.9. Note that when  $v_2^t = 0$ , the  $SR$  wave-pattern is well defined and the pressure at the contact discontinuity is intermediate between  $p_1$  and  $p_2$ . Note also that as  $v_2^t$  is increased, the wave-pattern gradually changes,  $p_3$  increases up until it becomes larger than  $p_1$ , signalling the transition to a  $2S$  wave-pattern.

Interestingly, the transition does not need to always produce a solution consisting of two shock

waves. Suppose, in fact, that the normal velocities are now chosen to be  $v_1^x = 0.0$ ,  $v_2^x = 0.5$ . We can repeat the considerations made above and start by examining the wave-pattern produced when there are zero tangential velocities. In this new setup,  $(v_{12}^x)_0 = -0.5$  and the right panel

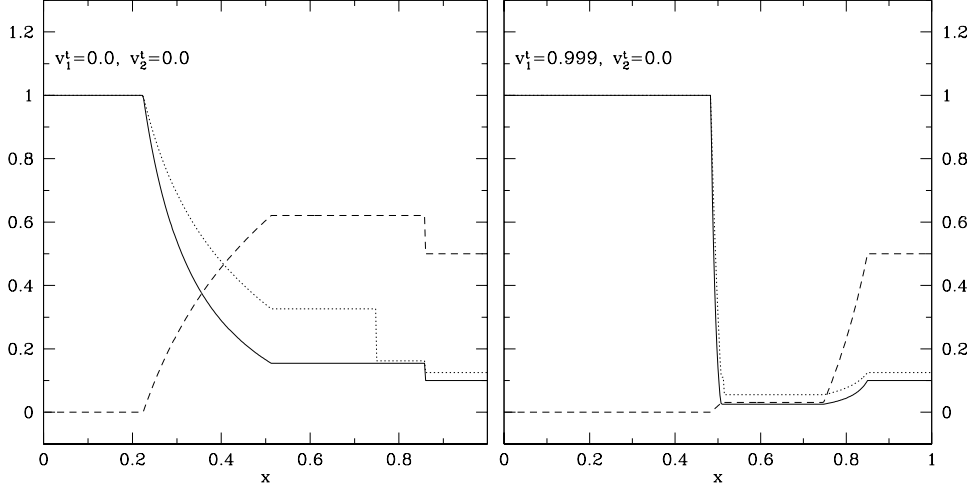


FIGURE 5. The same as in Fig. 3 but for models (h) and (n) in Table I. Also in this case the initial state vectors are identical except for the values of  $v_1^t$ . Note that in the right panel the left-propagating rarefaction wave covers a very small region of the flow and is closely followed by the contact discontinuity.

of Fig. 2 shows that the solution to the Riemann problem still falls in the  $SR$  branch (cf. dashed line), with the corresponding solution at a time  $t > 0$  being presented in the left panel of Fig. 5 (Note that the wave-patterns in Fig. 3 and 5 both consist of a shock and a rarefaction wave, but have alternating initial normal velocities.).

When nonzero tangential velocities are now considered in state 1, the right panel of Fig. 2 shows that  $(v_{12}^x)_0$  can fall in the  $2R$  branch, hence producing a wave-pattern consisting of two rarefaction waves moving in opposite directions. The solution to this Riemann problem is shown in right panel of Fig. 5 where we have chosen initial tangential velocities  $v_1^t = 0.999$  and  $v_2^t = 0.0$ . In this case too, it should be noted that, except for the tangential velocities, the solutions in the two panels of Fig. 5 have the same initial state-vectors but different intermediate ones.

In analogy with Fig. 4, we have collected in Fig. 6 a sequence of solutions for the pressure in which  $v_1^t$  is gradually increased from 0 to 0.999. Here too, when  $v_2^t = 0$ , the  $SR$  wave-pattern is well defined and the pressure at the contact discontinuity is intermediate between  $p_1$  and  $p_2$ . However, as  $v_1^t$  is increased, the wave-pattern gradually changes,  $p_3$  decreases until it becomes smaller than  $p_2$ , signalling the transition to a  $2R$  wave-pattern. Note that while this happens, the region of the flow covered by the rarefaction wave becomes progressively smaller.

In Table I we have summarized a few of the solutions shown in Figs. 4 and 6, presenting numerical values for all of the relevant quantities in the Riemann problem when different combinations of the tangential velocities are used.

To gain a better insight in these effects it can be instructive to consider how the velocities at which the various nonlinear waves propagate in the unperturbed media change when the tangential velocities  $v_1^t$  and  $v_2^t$  are varied separately. This information is contained in Fig. 7 in which different curves show the behaviour of the head and tail of a left-propagating rarefaction wave (i.e.  $\xi_{\text{tl}}^-$ ,  $\xi_{\text{hd}}^-$ ), of the head and tail of a right-propagating rarefaction wave (i.e.  $\xi_{\text{tl}}^+$ ,  $\xi_{\text{hd}}^+$ ), and of a left or a right-propagating shock wave (i.e.  $V_s^-$ ,  $V_s^+$ ). The left panel of Fig. 7, in particular,

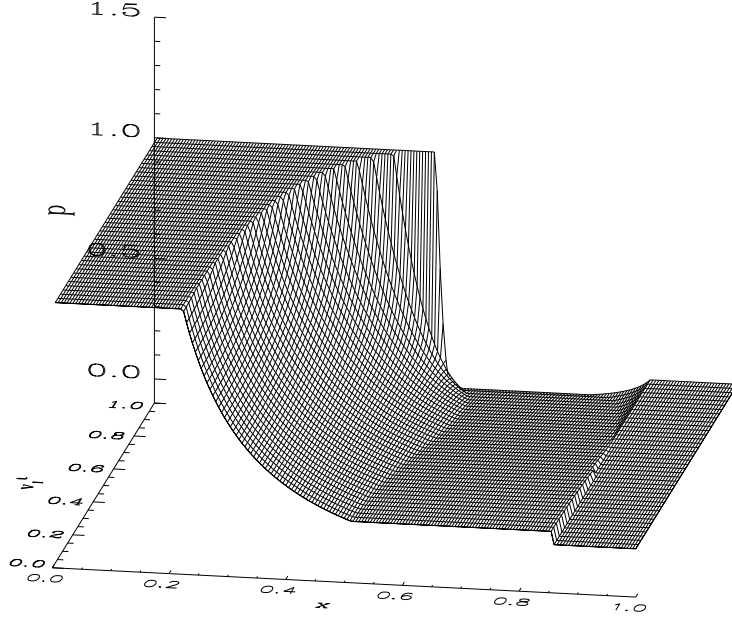


FIGURE 6. The same as in Fig. 4 but here the initial tangential velocity  $v_1^t$  is gradually increased from 0 to 0.999. The first and last solution of this sequence are also plotted in Fig. 5

shows the transition from a  $SR$  to a  $2S$  wave-pattern with the dotted line marking the value of  $v_2^t$  at which this occurs. Similarly, the right panel shows the transition from a  $SR$  to a  $2R$  wave-pattern and the dotted line is again used to mark the value of  $v_1^t$  distinguishing the two regions of the parameter space. A number of interesting features can be noted and some of these were pointed out also by Pons *et al* (2000). Firstly, the speed of the head of a rarefaction wave propagating towards a region of constant tangential velocity is constant, or, stated it differently,  $\xi_{hd}^-$  does not depend on  $v_2^t$ . Secondly, the velocity of the waves converges to zero if they propagate in regions with increasingly large tangential velocities. Thirdly, the values of  $v^t$  at which the speeds of the head and tail of the rarefaction wave coincide, mark the transition from one wave-pattern to another and are indicated with vertical dotted lines in Fig. 7.

As mentioned before, the appearance of these new relativistic effects is related to the behaviour of the function  $v_{12}^x = v_{12}^x(p_3)$  for different values of the initial tangential velocities and in particular to how the three branches composing the curve change under variation of  $v_{1,2}^t$ . As a result, the occurrence of these effects can be recast into the study of the dependence of  $(\tilde{v}_{12}^x)_{2S}$ ,  $(\tilde{v}_{12}^x)_{SR}$  and  $(\tilde{v}_{12}^x)_{2R}$  on the tangential velocities. Using expressions (4.5), (4.10), and (4.12), this dependence can be summarised as follows

$$(\tilde{v}_{12}^x)_{2S} = (\tilde{v}_{12}^x)_{2S}(v_2^t), \quad (\tilde{v}_{12}^x)_{SR} = (\tilde{v}_{12}^x)_{SR}(v_1^t), \quad (\tilde{v}_{12}^x)_{2R} = (\tilde{v}_{12}^x)_{2R}(v_1^t, v_2^t), \quad (5.1)$$

and can be best studied by considering the limits of  $(\tilde{v}_{12}^x)_{2S}$ ,  $(\tilde{v}_{12}^x)_{SR}$  and  $(\tilde{v}_{12}^x)_{2R}$  when  $W_{1,2} \rightarrow \infty$ . In the case of a  $2S$  wave-pattern, expression (4.5) simply indicates that

$$\lim_{W_2 \rightarrow \infty} (\tilde{v}_{12}^x)_{2S} = 0. \quad (5.2)$$

This result is also shown in the left panel of Fig. 2, where the right solid dot converges to zero as  $W_2 \rightarrow \infty$ , while the left one does not vary. The limit (5.2) can also be used to deduce that for

Model	$v_1^x$	$v_2^x$	$v_1^t$	$v_2^t$	$p_*$	$v_*^x$	$\rho_3$	$\rho_{3'}$	wave-pattern
(a)	0.5	0.0	0.0	0.000	0.597	0.640	0.734	0.342	SR
(b)	0.5	0.0	0.0	0.300	0.621	0.631	0.751	0.349	SR
(c)	0.5	0.0	0.0	0.500	0.673	0.611	0.788	0.364	SR
(d)	0.5	0.0	0.0	0.700	0.787	0.570	0.866	0.394	SR
(e)	0.5	0.0	0.0	0.900	1.150	0.455	1.088	0.474	2S
(f)	0.5	0.0	0.0	0.990	2.199	0.212	1.593	0.647	2S
(g)	0.5	0.0	0.0	0.999	3.011	0.078	1.905	0.750	2S
(h)	0.0	0.5	0.000	0.0	0.154	0.620	0.326	0.162	SR
(i)	0.0	0.5	0.300	0.0	0.139	0.594	0.306	0.152	SR
(j)	0.0	0.5	0.500	0.0	0.115	0.542	0.274	0.136	SR
(k)	0.0	0.5	0.700	0.0	0.085	0.450	0.228	0.113	2R
(l)	0.0	0.5	0.900	0.0	0.051	0.280	0.168	0.084	2R
(m)	0.0	0.5	0.990	0.0	0.031	0.095	0.123	0.061	2R
(n)	0.0	0.5	0.999	0.0	0.026	0.031	0.110	0.052	2R

TABLE 1. Solution of the modified Sod's problem at  $t = 0.4$ . All models refer to an ideal EOS with  $\gamma = 5/3$  and share the same values of pressure and rest-mass density:  $p_1 = 1.0$ ,  $\rho_1 = 1.0$ ,  $p_2 = 0.1$ ,  $\rho_2 = 0.125$ . The only differences present in the problems considered are in the normal relative velocity and in the tangential velocities. These quantities are reported in the first three columns, while the remaining ones show a few relevant quantities of the solution in the newly formed region as well as the wave pattern produced.

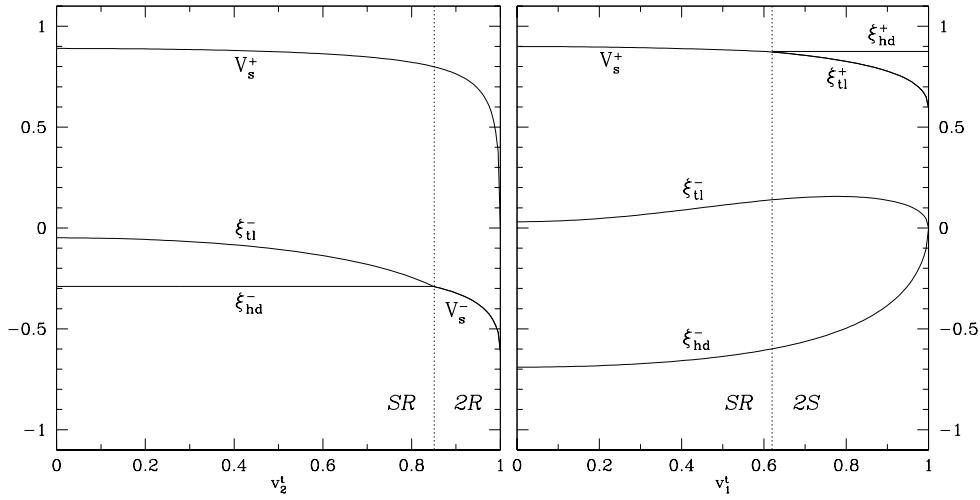


FIGURE 7. Velocities of the various nonlinear waves when the tangential velocities  $v_1^t$  and  $v_2^t$  are varied separately. The initial conditions are those of Sod's problem and the different curves refer to the head and tail of a left-propagating rarefaction wave (i.e.  $\xi_{tl}^-$ ,  $\xi_{hd}^-$ ), to the head and tail of a right-propagating rarefaction wave (i.e.  $\xi_{tl}^+$ ,  $\xi_{hd}^+$ ), and to a left or a right-propagating shock wave (i.e.  $V_s^-$ ,  $V_s^+$ ).

any  $(v_{12}^x)_0 > 0$ , there exists a value  $\bar{W}_2$  of  $W_2$  such that

$$(v_{12}^x)_0 > (\tilde{v}_{12}^x)_{2S} \quad \text{for } W_2 > \bar{W}_2. \quad (5.3)$$

A direct consequence of (5.3) is that given a Riemann problem having initial state vectors with

positive relative normal-velocity and producing a  $SR$  wave-pattern, it is always possible to transform it into a  $2S$  wave-pattern by increasing the value of the initial tangential velocity in the state of initial lower pressure.

In the case of a  $SR$  wave-pattern we refer to (4.10) to notice that in the limit of  $W_1 \rightarrow \infty$  the integrand vanishes ( $\mathcal{A}_1 \rightarrow \infty$ ) and therefore:

$$\lim_{W_1 \rightarrow \infty} (\tilde{v}_{12}^x)_{SR} = 0 . \quad (5.4)$$

As for the previous one, the limit (5.4) can be deduced from the right panel of Fig. 2, where the left solid dot converges to zero as  $W_1 \rightarrow \infty$ , while the right one does not vary. Also in this case the limit (5.4) can be used to conclude that for any  $(v_{12}^x)_0 < 0$ , there exists a value  $\bar{W}_1$  of  $W_1$  such that

$$(v_{12}^x)_0 < (\tilde{v}_{12}^x)_{SR} \quad \text{for } W_1 > \bar{W}_1 , \quad (5.5)$$

and therefore causing an initial  $SR$  wave-pattern solution to become a  $2R$  one as a consequence of an increased tangential velocity in the state of initial higher pressure<sup>†</sup>.

Overall, expressions (5.2) and (5.4) indicate that for tangential velocities assuming increasingly larger values, the  $SR$  branch of the  $v_{12}^x$  curve spans a progressively smaller interval of relative normal-velocities. When the tangential velocities reach their asymptotic values, the  $SR$  branch reduces to a point. In practice, therefore, the main effect introduced by relativistic tangential velocities in a Riemann problem is that of disfavoured the occurrence of a wave-pattern consisting of a shock and a rarefaction wave.

For completeness we also report the limit of the relative normal-velocity marking the branch of two rarefaction waves separated by vacuum. In this case, the limit is taken for both  $W_1$  and  $W_2$  tending to infinity, and using (4.13)-(4.14) yields

$$\lim_{W_{1,2} \rightarrow \infty} (\tilde{v}_{12}^x)_{2R} = 0 . \quad (5.6)$$

Because the effects discussed in this Section have a purely special relativistic origin they might conflict with our physical intuition, especially when the latter is based on the knowledge of the Riemann problem in Newtonian hydrodynamics. However, the behaviour reported here is typical of those special relativistic phenomena involving Lorentz factors including also tangential velocities. A useful example in this respect is offered by the relativistic transverse-Doppler effect, in which the wavelength of a photon received from a source moving at relativistic speeds changes also if the source has a velocity component orthogonal to the direction of emission of the photon (Rindler, 1980). In this case too, a Lorentz factor including the transverse velocity is responsible for the effect.

Finally, it should be pointed out that there exists a set of initial conditions for which these new relativistic effects cannot occur. These initial conditions are those in which  $v_1^x = v_2^x$  as in the classic ‘‘shock-tube’’ problem, where  $v_1^x = 0 = v_2^x$ . In this case, in fact,  $(v_{12}^x)_0 = 0$  and, because of the limits (5.2) and (5.4), the solution of the Riemann problem will be given by a wave-pattern consisting of a shock and a rarefaction wave, independently of the values of the tangential velocities.

## 6. Conclusions

We have shown that an efficient solution of the exact Riemann problem in multidimensional relativistic flows can be obtained after exploiting the properties of the invariant expression for the relative normal-velocity between the two initial states. The new procedure proposed here is the natural extension of a similar method presented for the exact solution of the Riemann problem

<sup>†</sup> Note that it is not possible to provide analytic expressions for  $\bar{W}_2$  nor for  $\bar{W}_1$ .



in one-dimensional relativistic flows (Rezzolla & Zanotti, 2001). Using information contained in the initial state vectors, this approach predicts the wave-pattern that will be produced in the Riemann problem, determines the set of equations to be solved and brackets the interval in pressure where the solution should be sought. Because logically straightforward, this approach results into an algorithm which is very easy to implement numerically and work is now in progress to assess the computational speedup in multidimensional codes.

An important aspect of this strategy is that it naturally points out relativistic effects that can take place whenever the initial relative velocity normal to the initial surface of discontinuity is nonzero. When this is the case, in fact, the tangential velocities can affect the solution of the Riemann problem and cause a transition from one wave-pattern to another one. More specifically, by varying the tangential velocities on either side of the initial discontinuity while keeping the remaining state vectors unchanged, the nonlinear waves involved in the solution Riemann problem can change from rarefaction waves to shock waves and vice-versa. These effects have a purely relativistic nature, do not have a Newtonian counterpart and could be relevant in several astrophysical scenarios, such as those involving relativistic jets or  $\gamma$ -ray bursts, in which nonlinear hydrodynamical waves with large Lorentz factors and complex multidimensional flows are expected (Blandford 2002, Meszaros 2002).

As a final remark it is worth pointing out that while the content of this paper is focussed on special relativistic hydrodynamics and flat spacetimes, the local Lorentz invariance allows to extend the results discussed here also to curved spacetimes and general relativistic numerical calculations (Pons *et al* 1998, and Font 2000 for a review).

### Appendix A: Monotonicity of the relative velocity as function of $p_*$

This Appendix is devoted to the proof that  $v_{12}^x$  is a monotonic function of  $p_*$ ; as mentioned in the main text, this is an important property and the basis of our approach.

With our choice of considering the initial left state as the one with highest pressure, the proof of monotonicity will be obtained if we show that  $v_{12}^x$  is a monotonically *increasing* function of  $p_*$ . Indicating then with a  $'$  the first derivative with respect to  $p_*$  and dropping the upper index  $x$  in the notation for the normal velocities, it is straightforward to derive that the first derivative of expression (3.6) is given by

$$v'_{12} = \frac{v'_{1,c}(1 - v_{2,c}^2) - v'_{2,c}(1 - v_{1,c}^2)}{(1 - v_{1,c} v_{2,c})^2}. \quad (1)$$

A rapid look at expression (1) suggests that the proof that  $v_{12}^x$  is monotonically increasing will follow if it can be shown that  $v'_{1,c}$  and  $-v'_{2,c}$  are both positive. On the other hand, using equations (3.4) and (3.5), the proof of the monotonicity will follow from showing that  $(v_3^x)' < 0$  and  $(v_3^x)' > 0$ . While these inequalities must hold irrespectively of the nonlinear wave considered, the proofs will be different for the different waves considered.

In the case when a rarefaction wave is present, the proof is indeed straightforward. According to (3.16) and (3.19), in fact,  $(v^x)'$  across the rarefaction wave is negative when the rarefaction wave propagates towards the left [implying that  $(v_3^x)'$  is negative] and it is positive when the rarefaction wave propagates towards the right [implying that  $(v_3^x)'$  is positive].

If a shock wave is present, on the other hand, a proof for the most general case and in terms of simple algebraic relations and cannot be given. On the other hand, a rather simple analytic proof can be found in the simpler case in which  $v_1^x = v_2^x = 0$ ; while this is certainly not the most general case, numerical calculations have shown that the result holds in general. Consider therefore a shock wave propagating towards the left<sup>†</sup>; after lengthy but straightforward calculations it is

<sup>†</sup> A similar analysis can be repeated for the right-propagating shock wave

possible to show that

$$(v_3^x)' = \frac{H_1(V_s - v_1^x)(1 - V_s v_1^x) - H_1 \Delta p (1 - (v_1^x)^2) V_s' - V_s' (\Delta p)^2}{[H_1(V_s - v_1^x) + \Delta p V_s]^2}, \quad (2)$$

where we have set  $H_1 \equiv h_1 \rho_1 W_1^2$  and  $\Delta p \equiv p - p_1 > 0$ , and where  $p$  is the pressure behind the shock. If we now impose that  $v_1^x = 0$ , we can write the derivative of (3.8) as

$$\frac{V_s'}{V_s} = \frac{J'}{J} \frac{\rho_1^2 W_1^2}{J^2 + \rho_1^2 W_1^2}. \quad (3)$$

Inserting (3) in (2) we can conclude that  $(v_3^x)'$  is negative if and only if

$$J(\rho_1^2 W_1^2 + J^2) h_1 - \rho_1 \Delta p J' (\rho_1 h_1 W_1^2 + \Delta p) < 0. \quad (4)$$

Using (3.13) to calculate  $J'$ , one finds that (4) can be written as

$$-\frac{\rho_1(H_1 - \Delta p)}{J^2} - 2h_1 < \frac{1}{\gamma(\gamma - 1)} \frac{\rho_1(H_1 + \Delta p)}{\rho^2} \left[ \frac{1}{\epsilon} - \gamma(\gamma - 2) \right], \quad (5)$$

where  $\rho$  and  $\epsilon$  are the rest-mass density and the specific internal energy behind the shock front. Because the right hand side of (5) is always positive for any  $\gamma \leq 2$ , the condition for monotonicity (5) will be satisfied if its left hand side is negative, i.e. if

$$-J^2 < -\rho_1 \frac{\Delta p - H_1}{2h_1} \equiv -\alpha. \quad (6)$$

At this point the proof can be continued graphically and making use of the Taub adiabat. In the plane  $(h/\rho, p)$ , in fact, the Taub adiabat (3.14) selects the points solutions of the hydrodynamical equations across a shock wave, therefore connecting the state ahead of the shock front with the one behind it. In Fig. 8, this curve is indicated with a solid line and we have indicated with the points A and B the states ahead (region 1) and behind (region 3) the shock front. Once an initial state A has been chosen, the mass flux will determine the point B of the Taub adiabat solution of the Rankine-Hugoniot relations. Because of this, the slope of the chord connecting the point A with B (shown as a dotted line in Fig. 8) is equal to  $-J^2$ . Indicated with a dashed line, Fig. 8 also shows the equivalent of the Taub adiabat passing through the state A but having mass flux equal to  $\alpha^{1/2}$ , i.e.

$$p = -\alpha \left( \frac{h}{\rho} - \frac{h_1}{\rho_1} \right) + p_1. \quad (7)$$

The point B' on such a curve represents the state behind the shock wave and, as it is clearly shown in Fig. 8, the slope of the chord AB' is always larger than the corresponding slope for the chord AB, thus stating that the condition (5) is indeed verified and that  $(v_3^x)'$  is therefore positive.

## Appendix B: An explicit expression for $\bar{V}_s$

In this Appendix we provide an explicit expression of the velocity of the shock wave propagating towards the right in the limit of  $p_3 \rightarrow p_1$  and when the fluid is ideal. This quantity, which is necessary to calculate the limiting relative velocity  $(\tilde{v}_{12}^x)_{2s}$  in equation (4.5), can be easily computed as [cf. eq. (3.8)]

$$\bar{V}_s = \frac{\rho_2^2 W_2^2 v_2^x + |J_{23'}| \sqrt{J_{23'}^2 + \rho_2^2 W_2^2 [1 - (v_2^x)^2]}}{\rho_2^2 W_2^2 + J_{23'}^2}, \quad (8)$$

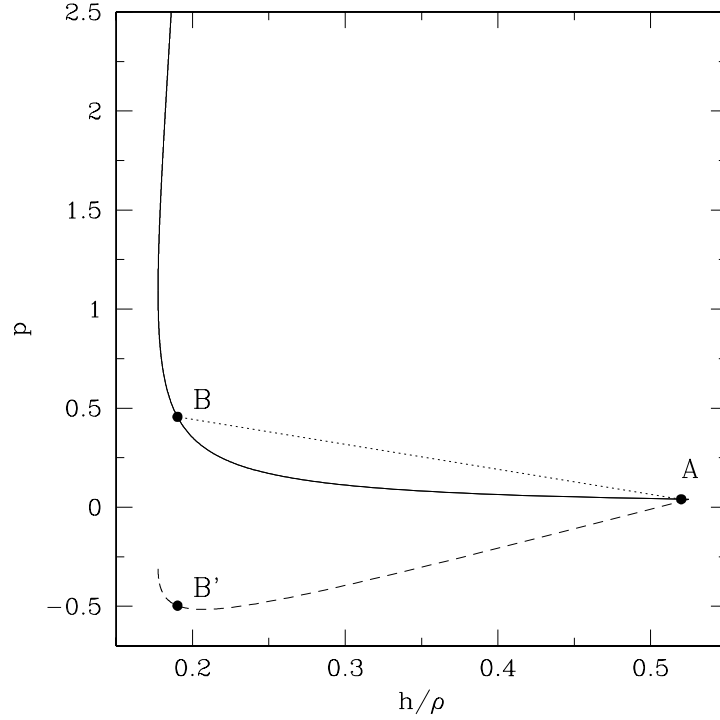


FIGURE 8. The solid curve represents the Taub adiabat and the points A and B on it the states ahead and behind a left-propagating shock wave. See the main text for a discussion.

where the mass flux  $J_{23'}$  is given by [cf. eq. (3.13)]

$$J_{23'}^2 = - \left( \frac{\gamma}{\gamma - 1} \right) \frac{p_1 - p_2}{h_{3'}(h_{3'} - 1)/p_1 - h_2(h_2 - 1)/p_2}, \quad (9)$$

and where, finally,  $h_{3'}$  is the positive root of the Taub adiabat (3.14) in the limit of  $p_3 \rightarrow p_1$ , i.e.

$$h_{3'} = \frac{(\sqrt{\mathcal{D}} - 1)(\gamma - 1)(p_1 - p_2)}{2[(\gamma - 1)p_2 + p_1]}. \quad (10)$$

The quantity  $\mathcal{D}$  in the root (10) is just a shorthand for

$$\mathcal{D} = 1 - 4\gamma p_1 \frac{(\gamma - 1)p_2 + p_1}{(\gamma - 1)^2(p_1 - p_2)^2} \left[ \frac{h_2(p_2 - p_1)}{\rho_2} - h_2^2 \right]. \quad (11)$$

It is a pleasure to thank J. C. Miller and J. M<sup>a</sup> Ibáñez for useful discussions and comments. Financial support for this research has been provided by the Italian MIUR and by the EU Programme “Improving the Human Research Potential and the Socio-Economic Knowledge Base” (Research Training Network Contract HPRN-CT-2000-00137). J.A.P. is supported by the Marie Curie Fellowship No. HPMF-CT-2001-01217.

#### REFERENCES

ANILE, A. M. 1989, *Relativistic Fluids and Magneto-Fluids: with Applications in astrophysics and plasma physics*, Cambridge University Press

- ANILE, A. M. AND RUSSO, G., 1987A, Corrugation stability for plane relativistic shock waves, *Phys. Fluids*, **29**, 2847
- ANILE, A. M. AND RUSSO, G., 1987B, Linear stability for plane relativistic shock waves, *Phys. Fluids*, **30**, 1045
- BLANDFORD, R. D. 2002, Black Holes and Relativistic Jets *Prog. of Theor. Phys. Supp.*, **143**, in press, astro-ph/0110394
- CHANDRASEKHAR, S. 1961, *Hydrodynamic and Hydromagnetic Stability*, Dover Pub. Inc., NY
- FONT, J. A. 2000 Numerical Hydrodynamics in General Relativity, *Living Reviews in Relativity*, Vol 3, 2.
- GODUNOV, S. K. 1959, A Finite Difference Method for the Numerical Computation and Discontinuous Solutions of the Equations of Fluid Dynamics, *Mat. Sb.*, **47**, 271.
- IBAÑEZ, J. M., MARTÍ, J. M. 1999, Riemann Solvers in relativistic astrophysics, *J. Comp. Appl. Math.* **109**, 173.
- LANDAU, L. D. AND LIFSHITZ, E. M. 1987, *Fluid Mechanics (Second Edition)*, Pergamon.
- LEVEQUE, R. J. 1992, *Numerical Methods for Conservation Laws*, Birkhauser
- KOENIGL, A., 1980, Relativistic gasdynamics in two dimensions, *Phys. Fluids* **23**, 1083.
- MARTÍ, J.M., IBAÑEZ, J. M., MIRALLES, J. A. 1991, Numerical relativistic hydrodynamics: local characteristic approach, *Phys. Rev. D* **43**, 3794.
- MARTÍ, J.M. & MÜLLER, E. 1994, The Analytical Solution of the Riemann Problem in Relativistic Hydrodynamics, *J. Fluid Mech.*, **258**, 317.
- MARTÍ, J.M. & MÜLLER, E. 1999 Numerical Hydrodynamics in Special Relativity, *Living Reviews in Relativity*, Vol 2, 3
- MESZAROS, P. 2002 Theories of Gamma-Ray Bursts *Annu. Rev. Astron. Astrophys.* **40** in press, astro-ph/0111170
- PONS, J.A., FONT, J.A., MARTÍ, J.M., IBAÑEZ, J.M. & MIRALLES, J.A. 1998, General Relativistic Hydrodynamics with Special Relativistic Riemann Solvers, *Astron. Astroph.* **339**, 638.
- PONS, J.A., MARTÍ, J.M., MÜLLER, E. 2000, The exact solution of the Riemann problem with nonzero tangential velocities in relativistic hydrodynamics *J. Fluid Mech.* **422**, 125.
- PRESS, W. H., TEUKOLSKY, S. A. VETTERLING, W. T., FLANNERY, B. P., 1992, *Numerical Recipes in Fortran 77*, Cambridge University Press, Second Ed.
- REZZOLLA, L. & ZANOTTI, O. 2001 An Improved Exact Riemann Solver for Relativistic Hydrodynamics, *J. Fluid Mech.* **449**, 395.
- REZZOLLA, L. & ZANOTTI, O. 2002 New Relativistic Effects in the Dynamics of Nonlinear Hydrodynamical Waves, *submitted*
- RINDLER, W. *Introduction to Special Relativity*, Clarendon Press, New York (1982)]
- RUSSO, G., 1988 Stability Properties of relativistic shock waves: Applications, *ApJ*, **334**, 707.
- SOD, G. A. 1978, A Survey of Several Finite Difference Methods for Systems of Nonlinear Hyperbolic Conservation Laws, *J. Comp. Phys.*, **27**, 1.
- SMOLLER, J. AND TEMPLE, B., 1993 Global Solutions of the Relativistic Euler Equations, *Commun. Math. Phys.*, **156**, 67.
- THORNE, K. S., 1973, Relativistic Shocks: the Taub Adiabatic *ApJ*, **179**, 897.
- TAUB, A. H., 1948, Relativistic Rankine-Hugoniot Relations, *Phys. Rev.*, **74**, 328.
- TORO, E. 1997, *Riemann Solvers and Numerical Methods for Fluid Dynamics*, Springer.